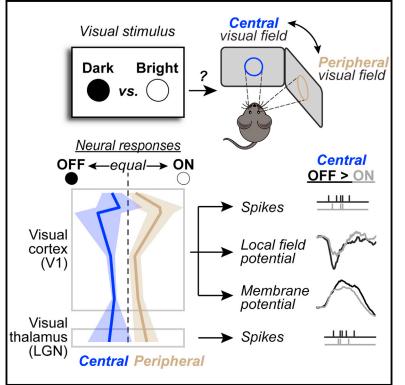# Spatial modulation of dark versus bright stimulus responses in the mouse visual system

Graphical abstract

Authors

Brice Williams, Joseph Del Rosario, Tomaso Muzzu, ..., Lisa Meyer-Baese, Aman B. Saleem, Bilal Haider

Correspondence

bilal.haider@bme.gatech.edu

In brief

Visual system neurons respond to both bright and dark stimuli (ON and OFF responses); it remains unclear which of these dominate mammalian vision. Williams et al. measure these responses across visual cortex and thalamus in awake mice and find that stimuli in the central visual field drive stronger OFF responses than stimuli in the far periphery.

Highlights

- Dark stimuli in the central visual field drive strong OFF responses in awake mice

- Dark and bright stimuli in the periphery drive more balanced OFF and ON responses

- LFP and membrane potential responses in binocular V1 show clear OFF dominance

- ON/OFF responses in V1 and lateral geniculate (LGN) show retinotopic alignment

Report

Spatial modulation of dark versus bright stimulus responses in the mouse visual system

Brice Williams,[1] Joseph Del Rosario,[1,3] Tomaso Muzzu,[2,3] Kayla Peelman,[1,3] Stefano Coletta,[1,3] Edyta K. Bichler,[1] Anderson Speed,[1] Lisa Meyer-Baese,[1] Aman B. Saleem,[2] and Bilal Haider[1,4,5,*]

[1]Biomedical Engineering, Georgia Institute of Technology & Emory University, Atlanta, GA, USA
[2]UCL Institute of Behavioural Neuroscience, Department of Experimental Psychology, University College London, London WC1H 0AP, UK
[3]These authors contributed equally
[4]Twitter: @haiderlab
[5]Lead contact
*Correspondence: bilal.haider@bme.gatech.edu
https://doi.org/10.1016/j.cub.2021.06.094

SUMMARY

A fundamental task of the visual system is to respond to both increases and decreases of luminance with action potentials (ON and OFF responses[1-4]). OFF responses are stronger, faster, and more salient than ON responses in primary visual cortex (V1) of both cats[5,6] and primates,[7,8] but in ferrets[9] and mice,[10] ON responses can be stronger, weaker,[11] or balanced[12] in comparison to OFF responses. These discrepancies could arise from differences in species, experimental techniques, or stimulus properties, particularly retinotopic location in the visual field, as has been speculated;[9] however, the role of retinotopy for ON/OFF dominance has not been systematically tested across multiple scales of neural activity within species. Here, we measured OFF versus ON responses across large portions of visual space with silicon probe and whole-cell patch-clamp recordings in mouse V1 and lateral geniculate nucleus (LGN). We found that OFF responses dominated in the central visual field, whereas ON and OFF responses were more balanced in the periphery. These findings were consistent across local field potential (LFP), spikes, and subthreshold membrane potential in V1, and were aligned with spatial biases in ON and OFF responses in LGN. Our findings reveal that retinotopy may provide a common organizing principle for spatial modulation of OFF versus ON processing in mammalian visual systems.

RESULTS AND DISCUSSION

OFF-dominant LFP in binocular V1, more balanced ON and OFF LFP in monocular V1

We first measured LFP responses in awake, head-fixed mice with laminar silicon probes. White or black bars (9° wide, vertical orientation, 0.1-s duration, inter-stimulus interval 0.3 s) appeared one at a time on isoluminant linearized LCD screens at multiple contrasts and positions across 150° of visual space spanning both monocular and binocular visual fields (Figure 1A). Bars presented within 20° of the vertical meridian evoked maximal LFP responses in binocular V1 (Figure 1B), and black bars elicited 48% larger responses than white bars at the center of the receptive field (RF; Figure 1D). In contrast, recordings from monocular V1 revealed larger LFP responses to white rather than black bars in the RF (Figures 1C and 1E).

Binocular V1 LFP responses showed significant OFF dominance across recordings. We computed the signal-to-noise ratio (SNR, response amplitude normalized by standard deviation[8,13]), then $\log_{10}$ transformed the ratio of white versus black bar SNRs; a $\log_{10}$ ratio <0 indicates a preference for black bars (OFF dominance), while a ratio >0 indicates preference for white bars (ON dominance). Across all cortical layers (defined by CSD analysis; Figure S1), LFP responses in binocular V1 showed significant

OFF dominance (Figure 2A; p < 0.001 across all layers, sign test; n = 58 recordings, 6 mice; median RF locations 19.8° ± 7.1°). In monocular V1, however, LFP responses were more balanced between ON and OFF (Figure 2B; n = 36 recordings, 7 mice; median RF preference: 77.4° ± 8.5°). In both locations, higher contrast accentuated luminance polarity preferences (Figure S2), as in prior reports.[5] These differences were not due to differing RF sizes (p = 0.97; Figure S2H) and not due to uneven sampling or binning into two groups, since there was a significant correlation between log ratio and L4 RF eccentricity across recordings (r = 0.53; p < 0.001; Figure S2G). Cumulative responses across layers of binocular V1 showed significant OFF dominance (Figure 2C; 86% of log ratios < 0; p < 0.001; sign test), whereas monocular V1 showed more balanced ON and OFF responses (57% of log ratios > 0; p = 0.38, sign test). Population responses in binocular V1 clearly showed significantly greater OFF responsiveness than monocular V1 (p < 0.001; two-sample, one-sided Kolmogorov-Smirnov test, unless otherwise noted).
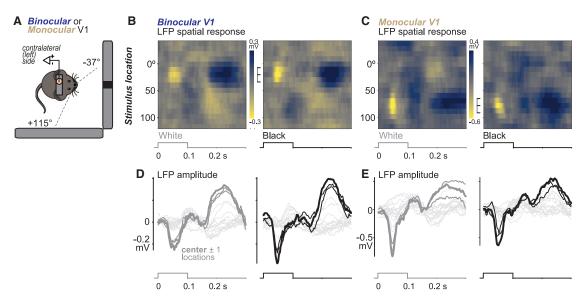
Spikes in binocular versus monocular V1 show spatial biases in ON/OFF dominance

Action potentials in these same recordings showed similar trends as LFP. We focused our analysis on regular spiking (RS) putative excitatory neurons across all layers (Figure S3). Peak

Figure 1. Black versus white stimulus responses in binocular versus monocular V1

(A) Head-fixed awake mice viewed black and white bars (9° wide, full screen height) presented across 150° of azimuthal visual space. Bars appeared one at a time at randomized location, contrast, and polarity. Vertical meridian defined as 0°, bars displayed from −37 to 115°. Neural activity recorded simultaneously with linear 32-channel silicon probe in binocular or monocular regions of primary visual cortex (V1).

(B) Example local field potential (LFP) responses in binocular V1 evoked by white (left) or black (right) bars appearing across azimuthal locations (ordinate). Median LFP responses to each bar presentation per location calculated across channels to create space-time receptive field (RF) maps. Brighter colors indicate depth negative LFP (activation). Maximum activation for black bars at 20°. Brackets span best three stimulus locations (center ± 1 locations) for the recording. Stimulus timing shown below maps (abscissa).

(C) Same as (B), for a recording from monocular V1. Maximum activation for white bars at 77°.

(D) Median LFP responses across channels to white (left) and black (right) bars for binocular recording in (B). Best stimulus location (center) defined by largest average evoked LFP response (thick trace). Responses to stimuli at the two adjacent (± 1) locations shown in thin bold traces, responses at all other locations shown in light gray. Peak binocular response 48% ± 27% (± SD) larger for black (−0.38 mV) than white (−0.26 mV) bar at same location.

(E) Same as (D), for monocular recording in (C). Peak monocular LFP response 31% ± 23% larger for white bars (−0.83 mV) than black bar responses at same location (−0.64 mV). See also Figures S1 and S2.

SNRs captured onset responses in 90% of all units (Figure S1). In monocular V1, RS neurons showed significant ON dominance (Figure 3A; 62% with log ratios > 0; n = 69; p = 0.035, sign test), while binocular V1 showed more balanced ON and OFF responses (53% with log ratios >0; n = 52; p = 0.78, sign test). Despite these spatial biases, there was not a significant difference between binocular and monocular populations (p = 0.078).

Similar spatial biases were evident in ON/OFF responses elicited by sparse black or white squares. In an independent set of experiments that projected black or white squares (10°, 0.1-s duration) onto a demispherical dome,[14] binocular and monocular V1 populations individually did not differ in ON versus OFF responses (binocular: 69% of log ratios < 0; p = 0.27; monocular: 61% > 0; p = 0.41), but binocular V1 neurons showed significantly greater OFF responsiveness than in monocular V1 (Figure 3B; n = 36; p = 0.015, Kolmogorov-Smirnov test). These findings reveal that neurons in binocular V1 show greater bias toward OFF responsiveness in spikes than those in monocular V1, but with considerable response heterogeneity within each population.
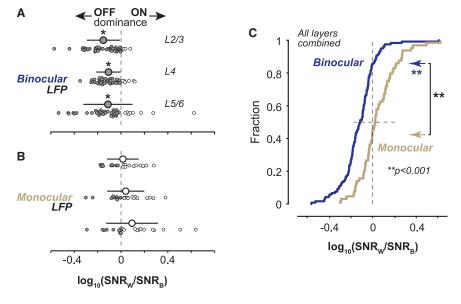
Motivated by these findings, we analyzed the publicly available Allen Brain Institute mouse V1 database.[15] Consistent with our findings, we found that binocular RS neurons (n = 978) were significantly OFF dominated (Figure S3C; 54% of neurons with log ratios < 0; p < 0.001), but so were monocular RS neurons

(n = 834; 56% with log ratios < 0; p < 0.001), with no difference between the two groups (p = 0.78). We reasoned that monocular OFF-dominant responses could arise from two key features of these experiments: (1) visual responses were evoked by sustained (0.25 s) full screen flashes, and (2) neurons were isolated with high-density Neuropixels probes. We directly tested both factors in our experiments and found these did not lead to OFF dominance in monocular V1 neurons: monocular V1 spikes showed ON/OFF-balanced or ON-dominant responses to full screen flashes (Figure S3). These controls bolstered consistency within our experimental conditions, so we next wondered if spatial biases were visible upstream in lateral geniculate nucleus (LGN).

Spikes in LGN show similar spatial biases in ON/OFF responses as those in V1

Spatial biases in LGN ON/OFF responses were aligned with those in V1. We targeted silicon probes to dorsal LGN in awake mice and measured responses to brief, small black or white squares (7° or 15°; see Figure S4 for RFs).[16] LGN neurons with RFs in the binocular visual field showed balanced ON and OFF responses as a population (Figure 3C; 57% of log ratios < 0; p = 0.4), but binocular LGN was significantly more OFF responsive than binocular V1 recorded in the same experimental conditions (Figure 3C inset; 47% of log ratios < 0; p = 0.03). We

Figure 2. OFF-dominant LFP in binocular V1, more balanced ON and OFF LFP in monocular V1

(A) $\log_{10}$ ratios of LFP SNR driven by full contrast white versus black stimuli, split by cortical layer (see Figure S1, S2). Binocular LFP responses significantly OFF dominated (log ratio < 0) across layers (L2/3: −0.15 ± 0.14, L4: −0.11 ± 0.10, L5/6: −0.11 ± 0.21; mean ± SD throughout figure; p < 0.001 for all, two-sided sign test; n = 58 recs in 6 mice).

(B) Same as (A), for monocular recordings. Monocular responses ON/OFF balanced across layers (L2/3: 0.016 ± 0.14, L4: 0.04 ± 0.16, L5/6: 0.094 ± 0.22; p = 0.82, 0.83, 0.52, two-sided sign test; n = 36 recs in 7 mice).

(C) Binocular responses significantly OFF dominated (blue; −0.12 ± 0.16, p < 0.001, sign test), monocular responses ON/OFF balanced (gold; 0.051 ± 0.18, p = 0.38, sign test). Cumulative density function of log ratios in (A) and (B) combined across layers. Binocular population significantly more OFF responsive than monocular (p < 0.001, Kolmogorov-Smirnov test). Arrows aligned to fraction of log ratios < 0 for each population (Binoc., 86%; Monoc., 45%). All data from awake mice trained in visual detection tasks. See also Figures S1 and S2.

interpret this difference between LGN and V1 to be driven by greater bias toward OFF responses in binocular LGN neurons (+7% bias toward OFF) rather than more ON-responsive binocular V1 neurons (+3% bias toward ON). In a next set of experiments, we found that LGN neurons with RFs in the monocular visual field were significantly ON dominant (70% of log ratios > 0; p < 0.001), but not significantly more than their counterparts in monocular V1 (also recorded in the same experimental conditions). Although both binocular and monocular LGN responses were recorded with small (7° or 15°) brief (0.1 s) squares, they were not recorded simultaneously within the same mice, nor from the same portions of LGN, warranting caution in a direct comparison of LGN populations. That said, OFF versus ON preferences in binocular versus monocular LGN populations were clearly significantly different from one another (p < 0.001; Figure S4). Overall, these findings in LGN predict that spatial biases in ON/OFF dominance should also be clearly visible in subthreshold activity of binocular versus monocular neurons in V1, examined next.
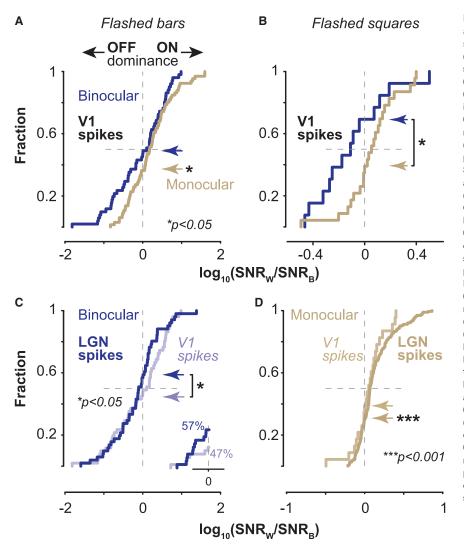
Spatial biases in ON/OFF membrane potential responses in V1

Subthreshold membrane potential (V_m) showed clear OFF dominance for binocular neurons, more balanced ON and OFF responses in monocular neurons, and clear differences between the two spatial locations. Using the exact same stimuli as LFP and spike recordings (Figures 1, 2, and 3A), we measured V_m and spikes with whole-cell patch-clamp recordings in L2/3 (both awake and anesthetized recordings; see STAR Methods). For neurons with RFs in binocular V1 (n = 13; Figures 4A and 4B), black bars evoked significantly greater depolarization and peak SNR (4.2 ± 0.1) than white bars (3.4 ± 0.1; p < 0.01, Wilcoxon rank sum test; Figure 4C). In contrast, neurons with RFs in monocular V1 (n = 19; Figures 4D and 4E) showed much larger average depolarization and significantly larger SNR for white (3.3 ± 0.03

versus black stimuli (2.2 ± 0.02; p < 0.001, Wilcoxon rank sum test; Figure 4F). V_m responses showed significant OFF dominance for the binocular population (Figure 4G; 77% of neurons with ratios < 0; n = 13; p = 0.031), but more balanced ON and OFF responses for the monocular population (68% with ratios >0, n = 19; p = 0.13), and significantly greater OFF responsiveness in binocular than monocular neurons (p = 0.03, Kolmogorov-Smirnov test). Binocular OFF dominance was most pronounced in neurons that emitted spikes (Figure 4H; 100% of binocular neuron V_m SNR ratios OFF dominated; p < 0.001), while monocular neurons that spiked showed more balanced in ON and OFF responses (66% of monocular neuron V_m SNR ratios > 0; p = 0.08). Accordingly, V_m in the binocular spiking population was significantly more OFF responsive than the monocular population (p < 0.001, Kolmogorov-Smirnov test). Finally, echoing our extracellular results, the subpopulations of spiking neurons within binocular (n = 9/13) and monocular (n = 18/19) V1 did not show clear ON or OFF dominance in spiking (binocular, p = 0.09; monocular, p = 0.11), but spike responses were significantly more OFF responsive in binocular versus monocular V1 neurons (Figure 4I; p = 0.043, Kolmogorov-Smirnov test; Figure S4).

Here, we revealed that ON and OFF responses in mouse V1 and LGN share considerable spatial biases based upon retinotopy. The central visual field shows stronger OFF responsiveness than the peripheral visual field. This spatial relationship pervaded multiple levels of neural activity in V1 across several independent experiments. Differences between binocular and monocular groups were apparent despite individual populations often showing more balanced ON and OFF responses. OFF dominance in binocular V1 LFP and membrane potential (V_m) showed the clearest spatial bias. Since LFP and V_m both reflect population activity, this indicates that ON/OFF biases in V1 emerge from large subnetworks of neurons that share luminance polarity preferences aligned by retinotopy. Our findings help resolve prior conflicting results and suggest common organizing

Figure 3. ON/OFF spike responses in V1 and LGN show retinotopically aligned spatial biases

(A) Regular spiking neurons (RS) in monocular V1 significantly ON dominant (gold, n = 69; log ratio: 0.21 ± 0.56, mean ± SD; 64% of data > 0; p = 0.035, sign test), but more ON and OFF balanced in binocular V1 (blue, n = 52; log ratio: −0.06 ± 0.65; 47% of data < 0; p = 0.78). Binocular versus monocular distributions not significantly different (p = 0.078, Kolmogorov-Smirnov test). SNRs peaked at 86 ± 30 ms (± SD) across entire dataset. Same experiments, mice, and stimuli as Figures 1 and 2. See Figure S3 for FS neurons.

(B) Responses to flashed squares (15°, 0.1 s) elicit ON/OFF-balanced responses in binocular (n = 13; log ratio: −0.099 ± 0.27, 69% of log ratios < 0; p = 0.27) and monocular V1 (n = 23; 0.055 ± 0.2, 61% of log ratios > 0; p = 0.41), but binocular population significantly more OFF responsive than monocular population (p = 0.015, Kolmogorov-Smirnov test). Full contrast black or white squares (9° or 15°, 0.1 s) projected onto spherical half dome in awake mice.

(C) Binocular LGN neurons ON/OFF balanced (−0.13 ± 0.59; 57% of log ratios < 0; p = 0.4; n = 51) but significantly more OFF responsive than binocular V1 neurons in (A) (inset: 47% of log ratios < 0; p = 0.03, Kolmogorov-Smirnov test; same binocular V1 neurons as A). All data recorded in awake mice as in (A), but with flashed squares (7°, 0.1 s), not bars.
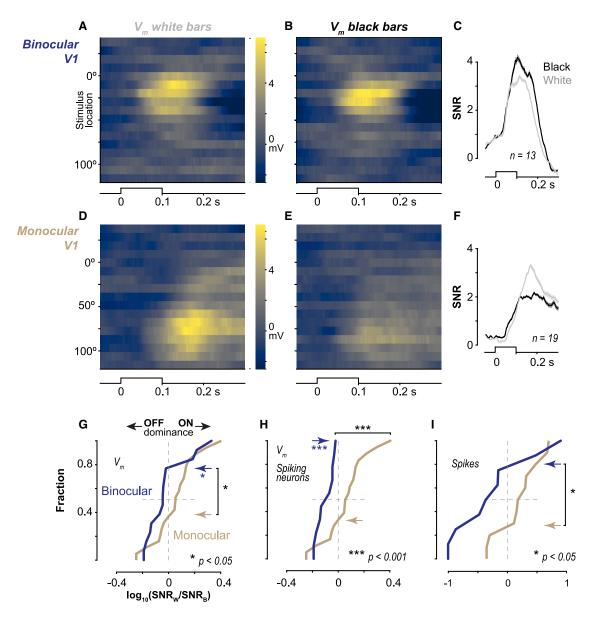
(D) Monocular LGN neurons significantly ON dominated (0.13 ± 0.22; 70% of log ratios > 0; p < 0.001; n = 193), but not more ON responsive than monocular V1 neurons in (B) (61% of log ratios > 0; p = 0.86, Kolmogorov-Smirnov test). All data recorded in awake mice as in (B) with flashed squares (15°, 0.1 s). See also Figures S3 and S4.

principles for spatial processing of luminance increments and decrements in mammalian visual systems. The spatial representation of ON versus OFF signals thus forms a critical substrate for visual perception.

Our findings of spatial biases in ON and OFF responses in mouse V1 echo and consolidate prior findings across several species, extend these to subthreshold measurements, and suggest a subcortical basis for these effects. Humans show enhanced behavioral responses for OFF signals in central vision.[17] Cat and primate V1 show OFF dominance in the central (<5°) region of binocular visual space.[6–8,13] Moreover, thalamic input to binocular V1 in cats is strongly OFF dominant, but ON responsiveness increases for peripheral visual space; indeed, this study established description of ON/OFF-balanced contributions in V1 outside the area centralis.[13] In ferret V1, peripheral visual field (~20°) responses show ON dominance.[9] Likewise, voltage dye responses in mouse V1 show ON dominance in the far monocular visual field;[10] however, Ca²⁺ responses in mouse V1 neurons with RFs in binocular V1 (20°–35° azimuth) show OFF dominance,[11] while those in monocular V1 show ON/OFF-balanced responses.[12] Our multi-scale electrophysiological measurements across nearly the entire visual hemifield resolve these discrepancies in mice and provide broad agreement with previous observations in other species, including preferential OFF processing in central vision[6,17,18] with increasing ON contributions in the periphery.[19] Together, our results suggest a simple organizing principle for mammalian visual cortex: spatial biases in ON/OFF responses are seeded by retinotopically aligned biases in LGN inputs. This perhaps explains why spatial biases in ON/OFF responses in V1 were most apparent in subthreshold membrane potential and LFP.

LFP, spikes, and Vm responses all showed stronger OFF responsiveness in binocular versus monocular V1 populations. The differences between populations were more apparent and consistent than ON or OFF dominance within individual populations. Importantly, we observed clear ON dominance only in subsets of monocular recordings and clear OFF dominance only in subsets of binocular recordings. In these binocular recordings, both LFP and Vm responses showed significant OFF dominance within population. Likewise, all monocular recordings (including LFP and Vm) showed more balanced ON and OFF responses, or ON dominance (spikes in LGN and V1). An exception to these

Figure 4. Spatial biases in ON/OFF membrane potential responses in V1

(A) Binocular V1 L2/3 membrane potential (V_m) responses to white bars (n = 13). Peak V_m depolarization (Δ6.3 mV) centered at 10°. Average pre-stimulus V_m subtracted from each neuron before averaging.

(B) Same neurons as (A), responses to black bars. Peak V_m depolarization (Δ6.7 mV) centered at 19°.

(C) Binocular V1 V_m signal-to-noise ratio (SNR, see STAR Methods) for black versus white bars at center (±1 locations) of receptive field (RF). Peak black SNR = 4.2 ± 0.1, white = 3.4 ± 0.1 (p < 0.01; Wilcoxon rank sum; mean ± SEM; n = 13 neurons).

(D–F) As in (A–C), for monocular V1 V_m response (n = 19 neurons). Peak depolarization for white bars (Δ6.8 mV) larger than for black bars (Δ3.3 mV), both centered at 77°. Peak black SNR = 2.2 ± 0.1, white = 3.2 ± 0.1 (p < 0.001; Wilcoxon rank sum).

(G) Log SNR ratios for binocular (blue) versus monocular (gold) neurons. Monocular V_m ON/OFF balanced (32% log ratios < 0; p = 0.13, sign test), binocular V_m significantly OFF dominant (77% log ratios < 0; p = 0.031) and significantly more OFF responsive than monocular V_m (p = 0.03, Kolmogorov-Smirnov test throughout G–I). See also Figure S4.

(H) Same as (G), for V_m of spiking neurons (n = 9 binocular, n = 18 monocular). Monocular neuron V_m ON/OFF balanced (p = 0.08), binocular neuron V_m significantly OFF dominated (p < 0.001), and significantly more OFF responsive than monocular neuron V_m (p < 0.001).

(I) Same as (H), for spikes. Monocular and binocular spikes balanced between ON and OFF responses (p = 0.11; p = 0.09), but binocular spikes significantly more OFF responsive than monocular (p = 0.04).

spatial biases was evident in the publicly available Allen Institute data, perhaps explainable by stimulus dependence,[20] but our recordings in monocular V1 with the same stimulus and recording probes as Allen experiments again elicited balanced or ON-dominant responses. Numerous other reasons could underlie these differences, such as sampling V1 sites with different

elevation, wavelength,[21] and spatial frequency preferences,[22] or differing behavioral conditions (such as training history, locomotion, and brain state) that modulate visual responses and are difficult to replicate exactly here.

We found that spatial biases in ON/OFF dominance of LFP permeated all cortical layers at a given spatial location. This is different from primates[7] and may be due to exquisite laminar organization of thalamic inputs in primates[23] versus more dispersed projections in mice.[24] Mouse V1 also lacks the organizing structure of ocular dominance, orientation, and ON/OFF subfield maps, as seen in other mammals.[9,25] However, retinotopic maps in mouse V1 are clear, and L2/3 neurons <200 microns from one another share highly localized and overlapping ON and OFF subfields,[12] providing a substrate for coherent local population responses to bright versus dark stimuli that were most visible in the LFP and V_m of L2/3. This suggests that LGN could provide V1 with a retinotopically aligned scaffold for biased luminance processing from central to peripheral visual space; indeed, this scaffold may ultimately arise from spatial gradients of ON versus OFF retinal ganglion cells in mice.[26,27]

We revealed that subthreshold synaptic responses in mouse V1 are selective for luminance polarity as a function of retinotopy. Subthreshold selectivity was most pronounced for cells that spiked. ON versus OFF selectivity may be amplified by spike threshold as with many other visual computations.[28] Patch-clamp recordings report every single spike and allow direct comparison of subthreshold responses and sparse spike responses; these comparisons revealed clearly greater OFF responsiveness in binocular versus monocular V1. Furthermore, in both V_m and LFP responses, we measured clear and strong OFF dominance in binocular V1 and more balanced ON and OFF responses in monocular V1 in entirely separate mice and experiments. Given the close relationship between LFP, V_m, and synaptic activity in mouse V1,[29] this suggests that presynaptic populations share coherent selectivity for both stimulus position and luminance polarity preference. This could ensure that ON and OFF computations in V1 also contain appropriate spatial signals for downstream targets.

ON/OFF dominance was less pronounced in spikes than LFP or V_m, for several potential reasons. First, unlike the inherently correlated population activity driving LFP and V_m, our single-neuron spike analysis did not consider population correlations, a topic for further study. Second, bars appeared at a single vertical orientation (and squares were unoriented), sub-optimal stimuli for many V1 neurons selective for other orientations. However, even sub-optimal stimuli depolarize membrane potential[28,30] and drive LFP responses that reflect local synaptic activity,[29,31] perhaps contributing to stronger ON/OFF dominance trends in LFP and V_m. Third, patch-clamp pipettes isolate cells regardless of activity levels, allowing measurements from the many cells that rarely spike.[32,33] Silicon probe recordings require large numbers of spikes to form clusters, necessarily favoring high firing rate and/or less selective cells that spike to both dark and bright stimuli, potentially oversampling ON/OFF balanced neurons. Statistically resolving exactly balanced versus ON/OFF dominant spike responses depends upon effect sizes and population sizes, and both will be constrained by the experimental technique. In light of these caveats, our independent datasets of V1 spikes (both extracellular and intracellular)

with comparable sampling constraints in monocular or binocular experiments broadly revealed greater OFF responsiveness in binocular versus monocular V1, consistent with LFP and V_m responses measured in the same experimental conditions.

In summary, we found that OFF responses are strongest in central visual space, but more balanced between ON and OFF in peripheral visual space. These results establish that OFF versus ON dominance in the mouse thalamocortical visual system varies as a function of retinotopy. Why might spatial modulation of OFF versus ON responses be beneficial for mice? Their peripheral vision encompasses a large monocular region, while binocular vision spans at least 40° of space that is prioritized during navigation,[34–36] perhaps underlying computation of self-motion versus visual motion.[37] Dark stimuli that drift or loom in binocular visual space elicit freezing versus fleeing,[35,38] and mice also use binocular vision for depth perception,[34] daytime foraging,[39,40] and insect hunting.[41–43] Even while stationary, mice use binocular vision with greatest perceptual sensitivity,[44] but attention can quickly improve sensitivity to stimuli in monocular visual space.[45] Thus, mice show several specializations in spatial visual processing and behavior,[45–47] including spatially biased ON/OFF processing as shown here. Future studies in mice will enable detailed investigation of the circuits and mechanisms driving a variety of spatial visual behaviors elicited by luminance increments and decrements, a fundamental aspect of vision.

STAR★METHODS

Detailed methods are provided in the online version of this paper and include the following:

- KEY RESOURCES TABLE
- RESOURCE AVAILABILITY
  - Lead contact
  - Materials availability
  - Data and code availability
- EXPERIMENTAL MODEL AND SUBJECT DETAILS
  - Experimental subjects—Haider lab
  - Experimental subjects—Saleem lab
  - Experimental subjects—Allen Institute
- METHOD DETAILS
  - Recordings
  - Visual stimuli
- QUANTIFICATION AND STATISTICAL ANALYSIS
  - Spike sorting
  - Receptive field (RF) map analysis

SUPPLEMENTAL INFORMATION

Supplemental information can be found online at https://doi.org/10.1016/j.cub.2021.06.094.

INCLUSION AND DIVERSITY

We worked to ensure sex balance in the selection of non-human subjects. One or more of the authors of this paper self-identifies as an underrepresented ethnic minority in science. One or more of the authors of this paper self-identifies as a member of the LGBTQ+ community. One or more of the authors of this paper received support from a program designed to increase minority representation in science. The author list of this paper includes contributors from the location where the research was conducted who participated in the data collection, design, analysis, and/or interpretation of the work.

REFERENCES

1. Joesch, M., Schnell, B., Raghu, S.V., Reiff, D.F., and Borst, A. (2010). ON and OFF pathways in Drosophila motion vision. Nature 468, 300–304. https://doi.org/10.1038/nature09545.

2. Schiller, P.H. (1995). The ON and OFF channels of the mammalian visual system. Prog. Retin. Eye Res. 15, 173–195. https://doi.org/10.1016/1350-9462(95)00009-7.

3. Field, G.D., and Chichilnisky, E.J. (2007). Information processing in the primate retina: circuitry and coding. Annu. Rev. Neurosci. 30, 1–30. https://doi.org/10.1146/annurev.neuro.30.051606.094252.

4. Kuffler, S.W. (1953). Discharge patterns and functional organization of mammalian retina. J. Neurophysiol. 16, 37–68. https://doi.org/10.1152/jn.1953.16.1.37.

5. Liu, K., and Yao, H. (2014). Contrast-dependent OFF-dominance in cat primary visual cortex facilitates discrimination of stimuli with natural contrast statistics. Eur. J. Neurosci. 39, 2060–2070. https://doi.org/10.1111/ejn.12567.

6. Jin, J., Wang, Y., Lashgari, R., Swadlow, H.A., and Alonso, J.M. (2011). Faster thalamocortical processing for dark than light visual targets. J. Neurosci. 31, 17471–17479. https://doi.org/10.1523/JNEUROSCI.2456-11.2011.

7. Xing, D., Yeh, C.I., and Shapley, R.M. (2010). Generation of black-dominant responses in V1 cortex. J. Neurosci. 30, 13504–13512. https://doi.org/10.1523/Jneurosci.2473-10.2010.

8. Yeh, C.I., Xing, D., and Shapley, R.M. (2009). "Black" responses dominate macaque primary visual cortex v1. J. Neurosci. 29, 11753–11760. https://doi.org/10.1523/Jneurosci.1991-09.2009.

9. Smith, G.B., Whitney, D.E., and Fitzpatrick, D. (2015). Modular Representation of Luminance Polarity in the Superficial Layers of Primary Visual Cortex. Neuron 88, 805–818. https://doi.org/10.1016/j.neuron.2015.10.019.

10. Polack, P.O., and Contreras, D. (2012). Long-range parallel processing and local recurrent activity in the visual cortex of the mouse.

J. Neurosci. 32, 11120–11131. https://doi.org/10.1523/JNEUROSCI.6304-11.2012.

11. Jimenez, L.O., Tring, E., Trachtenberg, J.T., and Ringach, D.L. (2018). Local tuning biases in mouse primary visual cortex. J. Neurophysiol. 120, 274–280. https://doi.org/10.1152/jn.00150.2018.

12. Smith, S.L., and Häusser, M. (2010). Parallel processing of visual space by neighboring neurons in mouse visual cortex. Nat. Neurosci. 13, 1144–1149. https://doi.org/10.1038/nn.2620.

13. Jin, J.Z., Weng, C., Yeh, C.I., Gordon, J.A., Ruthazer, E.S., Stryker, M.P., Swadlow, H.A., and Alonso, J.M. (2008). On and off domains of geniculate afferents in cat primary visual cortex. Nat. Neurosci. 11, 88–94. https://doi.org/10.1038/nn2029.

14. Muzzu, T., and Saleem, A.B. (2021). Feature selectivity explains mismatch signals in mouse visual cortex. bioRxiv. https://doi.org/10.1101/2021.04.12.439457.

15. Siegle, J.H., Jia, X., Durand, S., Gale, S., Bennett, C., Graddis, N., Heller, G., Ramirez, T.K., Choi, H., Luviano, J.A., et al. (2019). A survey of spiking activity reveals a functional hierarchy of mouse corticothalamic visual areas. bioRxiv. https://doi.org/10.1101/805010.

16. Siegle, J.H., Jia, X., Durand, S., Gale, S., Bennett, C., Graddis, N., Heller, G., Ramirez, T.K., Choi, H., Luviano, J.A., et al. (2021). Survey of spiking in the mouse visual system reveals functional hierarchy. Nature 592, 86–92. https://doi.org/10.1038/s41586-020-03171-x.

17. Komban, S.J., Alonso, J.M., and Zaidi, Q. (2011). Darks are processed faster than lights. J. Neurosci. 31, 8654–8658. https://doi.org/10.1523/Jneurosci.0504-11.2011.

18. Rekauzke, S., Nortmann, N., Staadt, R., Hock, H.S., Schöner, G., and Jancke, D. (2016). Temporal Asymmetry in Dark-Bright Processing Initiates Propagating Activity across Primary Visual Cortex. J. Neurosci. 36, 1902–1913. https://doi.org/10.1523/JNEUROSCI.3235-15.2016.

19. Chichilnisky, E.J., and Kalmar, R.S. (2002). Functional asymmetries in ON and OFF ganglion cells of primate retina. J. Neurosci. 22, 2737–2747.

20. Jansen, M., Jin, J., Li, X., Lashgari, R., Kremkow, J., Bereshpolova, Y., Swadlow, H.A., Zaidi, Q., and Alonso, J.M. (2019). Cortical Balance Between ON and OFF Visual Responses Is Modulated by the Spatial Properties of the Visual Stimulus. Cereb. Cortex 29, 336–355. https://doi.org/10.1093/cercor/bhy221.

21. Denman, D.J., Luviano, J.A., Ollerenshaw, D.R., Cross, S., Williams, D., Buice, M.A., Olsen, S.R., and Reid, R.C. (2018). Mouse color and wavelength-specific luminance contrast sensitivity are non-uniform across visual space. eLife 7, e31209. https://doi.org/10.7554/eLife.31209.

22. Zhang, X., An, X., Liu, H., Peng, J., Cai, S., Wang, W., Lin, D.T., and Yang, Y. (2015). The topographical arrangement of cutoff spatial frequencies across lower and upper visual fields in mouse V1. Sci. Rep. 5, 7734. https://doi.org/10.1038/srep07734.

23. Callaway, E.M. (1998). Local circuits in primary visual cortex of the macaque monkey. Annu. Rev. Neurosci. 21, 47–74. https://doi.org/10.1146/annurev.neuro.21.1.47.

24. Antonini, A., Fagiolini, M., and Stryker, M.P. (1999). Anatomical correlates of functional plasticity in mouse visual cortex. J. Neurosci. 19, 4388–4406.

25. Lee, K.S., Huang, X., and Fitzpatrick, D. (2016). Topology of ON and OFF inputs in visual cortex enables an invariant columnar architecture. Nature 533, 90–94. https://doi.org/10.1038/nature17941.

26. Bleckert, A., Schwartz, G.W., Turner, M.H., Rieke, F., and Wong, R.O. (2014). Visual space is represented by nonmatching topographies of distinct mouse retinal ganglion cell types. Curr. Biol. 24, 310–315. https://doi.org/10.1016/j.cub.2013.12.020.

27. Schroder, S., Steinmetz, N.A., Krumin, M., Pachitariu, M., Rizzi, M., Lagnado, L., Harris, K.D., and Carandini, M. (2020). Arousal Modulates Retinal Output. Neuron 107, 487–495.e9. https://doi.org/10.1016/j.neuron.2020.04.026.

28. Priebe, N.J., and Ferster, D. (2012). Mechanisms of neuronal computation in mammalian visual cortex. Neuron 75, 194–208. https://doi.org/10.1016/j.neuron.2012.06.011.

29. Haider, B., Schulz, D.P., Häusser, M., and Carandini, M. (2016). Millisecond Coupling of Local Field Potentials to Synaptic Currents in the Awake Visual Cortex. Neuron *90*, 35–42. https://doi.org/10.1016/j.neuron.2016.02.034.

30. Lien, A.D., and Scanziani, M. (2013). Tuned thalamic excitation is amplified by visual cortical circuits. Nat. Neurosci. *16*, 1315–1323. https://doi.org/10.1038/nn.3488.

31. Katzner, S., Nauhaus, I., Benucci, A., Bonin, V., Ringach, D.L., and Carandini, M. (2009). Local origin of field potentials in visual cortex. Neuron *61*, 35–41. https://doi.org/10.1016/j.neuron.2008.11.016.

32. Margrie, T.W., Brecht, M., and Sakmann, B. (2002). In vivo, low-resistance, whole-cell recordings from neurons in the anaesthetized and awake mammalian brain. Pflugers Arch. *444*, 491–498. https://doi.org/10.1007/s00424-002-0831-z.

33. Haider, B., Häusser, M., and Carandini, M. (2013). Inhibition dominates sensory responses in the awake cortex. Nature *493*, 97–100. https://doi.org/10.1038/nature11665.

34. Samonds, J.M., Choi, V., and Priebe, N.J. (2019). Mice Discriminate Stereoscopic Surfaces Without Fixating in Depth. J. Neurosci. *39*, 8024–8037. https://doi.org/10.1523/JNEUROSCI.0895-19.2019.

35. Wallace, D.J., Greenberg, D.S., Sawinski, J., Rulla, S., Notaro, G., and Kerr, J.N. (2013). Rats maintain an overhead binocular field at the expense of constant fusion. Nature *498*, 65–69. https://doi.org/10.1038/nature12153.

36. Meyer, A.F., O'Keefe, J., and Poort, J. (2020). Two Distinct Types of Eye-Head Coupling in Freely Moving Mice. Curr. Biol. *30*, 2116–2130.e6. https://doi.org/10.1016/j.cub.2020.04.042.

37. Saleem, A.B. (2020). Two stream hypothesis of visual processing for navigation in mouse. Curr. Opin. Neurobiol. *64*, 70–78. https://doi.org/10.1016/j.conb.2020.03.009.

38. De Franceschi, G., Vivattanasarn, T., Saleem, A.B., and Solomon, S.G. (2016). Vision Guides Selection of Freeze or Flight Defense Strategies in Mice. Curr. Biol. *26*, 2150–2154. https://doi.org/10.1016/j.cub.2016.06.006.

39. Daan, S., Spoelstra, K., Albrecht, U., Schmutz, I., Daan, M., Daan, B., Rienks, F., Poletaeva, I., Dell'Omo, G., Vyssotski, A., and Lipp, H.P. (2011). Lab mice in the field: unorthodox daily activity and effects of a dysfunctional circadian clock allele. J. Biol. Rhythms *26*, 118–129. https://doi.org/10.1177/0748730410397645.

40. Hut, R.A., Pilorz, V., Boerema, A.S., Strijkstra, A.M., and Daan, S. (2011). Working for food shifts nocturnal mouse activity into the day. PLoS ONE *6*, e17527. https://doi.org/10.1371/journal.pone.0017527.

41. Michaiel, A.M., Abe, E.T., and Niell, C.M. (2020). Dynamics of gaze control during prey capture in freely moving mice. eLife *9*, e57458. https://doi.org/10.7554/eLife.57458.

42. Hoy, J.L., Yavorska, I., Wehr, M., and Niell, C.M. (2016). Vision Drives Accurate Approach Behavior during Prey Capture in Laboratory Mice. Curr. Biol. *26*, 3046–3052. https://doi.org/10.1016/j.cub.2016.09.009.

43. Shang, C., Liu, A., Li, D., Xie, Z., Chen, Z., Huang, M., Li, Y., Wang, Y., Shen, W.L., and Cao, P. (2019). A subcortical excitatory circuit for sensory-triggered predatory hunting in mice. Nat. Neurosci. *22*, 909–920. https://doi.org/10.1038/s41593-019-0405-4.

44. Speed, A., Del Rosario, J., Burgess, C.P., and Haider, B. (2019). Cortical State Fluctuations across Layers of V1 during Visual Spatial Perception. Cell Rep. *26*, 2868–2874.e3. https://doi.org/10.1016/j.celrep.2019.02.045.

45. Speed, A., Del Rosario, J., Mikail, N., and Haider, B. (2020). Spatial attention enhances network, cellular and subthreshold responses in mouse visual cortex. Nat. Commun. *11*, 505. https://doi.org/10.1038/s41467-020-14355-4.

46. Saleem, A.B., Diamanti, E.M., Fournier, J., Harris, K.D., and Carandini, M. (2018). Coherent encoding of subjective spatial position in visual cortex and hippocampus. Nature *562*, 124–127. https://doi.org/10.1038/s41586-018-0516-1.

47. Wang, L., and Krauzlis, R.J. (2018). Visual Selective Attention in Mice. Curr. Biol. *28*, 676–685.e4. https://doi.org/10.1016/j.cub.2018.01.038.

48. Rossant, C., Kadir, S.N., Goodman, D.F.M., Schulman, J., Hunter, M.L.D., Saleem, A.B., Grosmark, A., Belluscio, M., Denfield, G.H., Ecker, A.S., et al. (2016). Spike sorting for large, dense electrode arrays. Nat. Neurosci. *19*, 634–641. https://doi.org/10.1038/nn.4268.

49. Pachitariu, M., Steinmetz, N., Kadir, S., Carandini, M., and Kenneth, D.H. (2016). Kilosort: realtime spike-sorting for extracellular electrophysiology with hundreds of channels. bioRxiv. https://doi.org/10.1101/061481.

50. Lopes, G., Farrell, K., Horrocks, E.A.B., Lee, C.-Y., Morimoto, M.M., Muzzu, T., et al. (2021). Creating and controlling visual environments using BonVision. eLife *10*, e65541. https://doi.org/10.7554/eLife.65541.

51. AllenBrainObservatory (2019). Neuropixels Visual Coding, Technical white paper, overview v1.0. brain-map.org.

52. Siegle, J.H., López, A.C., Patel, Y.A., Abramov, K., Ohayon, S., and Voigts, J. (2017). Open Ephys: an open-source, plugin-based platform for multi-channel electrophysiology. J. Neural Eng. *14*, 045003. https://doi.org/10.1088/1741-2552/aa5eea.

53. Jun, J.J., Steinmetz, N.A., Siegle, J.H., Denman, D.J., Bauza, M., Barbarits, B., Lee, A.K., Anastassiou, C.A., Andrei, A., Aydın, Ç., et al. (2017). Fully integrated silicon probes for high-density recording of neural activity. Nature *551*, 232–236. https://doi.org/10.1038/nature24636.

54. Pfeffer, C.K., Xue, M., He, M., Huang, Z.J., and Scanziani, M. (2013). Inhibition of inhibition in visual cortex: the logic of connections between molecularly distinct interneurons. Nat. Neurosci. *16*, 1068–1076. https://doi.org/10.1038/nn.3446.

55. Dräger, U.C. (1975). Receptive fields of single cells and topography in mouse visual cortex. J. Comp. Neurol. *160*, 269–290. https://doi.org/10.1002/cne.901600302.

56. Niell, C.M. (2015). Cell types, circuits, and receptive fields in the mouse visual cortex. Annu. Rev. Neurosci. *38*, 413–431. https://doi.org/10.1146/annurev-neuro-071714-033807.

STAR★METHODS

KEY RESOURCES TABLE

Reagent or resource	Source	Identifier
Deposited data		
Allen Institute Visual Coding database	The Allen Institute, see also.[15]	https://portal.brain-map.org/explore/circuits/visual-coding-neuropixels
Data structures and code to generate main results	Figshare.com	Database: https://doi.org/10.6084/m9.figshare.14852946
Experimental models: Organisms/strains		
Mouse B6PV^Cre	Jackson Laboratory	IMSR_JAX:017320
Mouse C57BL/6J	Jackson Laboratory	IMSR_JAX:000664
Mouse Ai32	Jackson Laboratory	IMSR_JAX:024109
Mouse Sst-IRES-Cre	Jackson Laboratory	IMSR_JAX:013044
Mouse Ai32 x Scnn1a-cre	Jackson Laboratory	IMSR_JAX:009613
Mouse CNTNAP2$^{-/-}$	Jackson Laboratory	IMSR_JAX:017482
Mouse Ai40	Jackson Laboratory	IMSR_JAX: 021188
Software and algorithms		
MATLAB	Mathworks, Inc.	https://www.mathworks.com
KlustaSuite	Original paper[48]	https://klusta.readthedocs.io/en/latest/
Kilosort	Original paper[49]	https://github.com/MouseLand/Kilosort

RESOURCE AVAILABILITY

Lead contact
All requests for resources should be directed to and will be fulfilled by Bilal Haider (bilal.haider@bme.gatech.edu).

Materials availability
This study did not generate new unique reagents or materials.

Data and code availability
Data and code for each figure will be deposited at DOI 10.6084/m9.figshare.14852946 and linked from the corresponding author's institutional webpage.

EXPERIMENTAL MODEL AND SUBJECT DETAILS

All procedures were approved by the Institutional Animal Care and Use Committee at the Georgia Institute of Technology and University College London and were in agreement with guidelines established by the National Institutes of Health, and The Animal (Scientific Procedures) Act 1986.

Experimental subjects—Haider lab
Detailed methods have been described previously.[44] Mice (5 – 8 weeks old; reverse light cycle individual housing; bred in house) were chronically implanted with a stainless steel headplate with a recording chamber during isoflurane (1%–2%) anesthesia. After implant surgery mice recovered for 3 days before experimentation. All silicon probe recordings in V1 were from mice that were trained over several weeks to perform a visual spatial detection task,[45] except those in Figures S3D–S3F.

Recordings in Haider lab used male and female mice. Across all labs, there was no allocation strategy for selecting subjects, since there were no comparisons between experimental groups.

Mouse Strain	n = mice [probes; patch]	n = recordings [probes; patch]	RRID
B6PV^Cre	[3;1]	[31;1]	IMSR_JAX:017320
C57BL/6J	[8;0]	[27;0]	IMSR_JAX:000664

(Continued on next page)

Continued

Mouse Strain	n = mice [probes; patch]	n = recordings [probes; patch]	RRID
Ai32	[1;0]	[13;0]	IMSR_JAX:024109
Sst-IRES-Cre	[1;1]	[5;2]	IMSR_JAX:013044
Ai32 x B6PV[Cre]	[3;7]	[26;10]	See above
Ai32 x Sst-IRES-Cre	[3;2]	[62,8]	See above
Ai32 x Scnn1a-cre	[1;4]	[2;7]	IMSR_JAX:009613
CNTNAP2$^{-/-}$	[0;1]	[0;1]	IMSR_JAX:017482
Ai40	[0;1]	[0;1]	IMSR_JAX: 021188
Uncertain genotype	[0;1]	[0;2]	–

Experimental subjects—Saleem lab

Detailed methods have been described previously.[50] Mice were implanted with a custom-built stainless steel metal plate under iso-flurane anesthesia. The area above the left visual cortex was kept accessible for electrophysiological recordings.

Recordings in Saleem lab used male mice.

Mouse Strain	n = mice	n = recording sessions	RRID
C57BL/6J	9	32	See above

Experimental subjects—Allen Institute

Recordings from the Allen Institute – Visual Coding database are fully detailed elsewhere.[51] Both male and female mice were used, and only one mouse was used per recording.

Mouse Strain	n = mice	n = neurons	RRID
C57BL/6J	26	1444	See above
Ai32 x B6PV[Cre]	5	195	See above
Ai32 x Sst-IRES-Cre	10	504	See above
Ai32 x Vip-IRES-Cre	6	347	See above

METHOD DETAILS

Recordings

Haider lab—V1 extracellular

At the conclusion of training, a small craniotomy (100-400 microns) was opened over monocular or binocular V1 during isoflurane anesthesia. Mice were allowed 3 h of recovery before awake acute recordings. Single shank linear 32 site silicon probes (Neuronexus, A1x32) were used to record neural activity across cortical layers in head-fixed stationary mice resting comfortably in a semi-enclosed plastic tube. The electrode was typically advanced to 1 mm below the dura, and the site was covered in sterile artificial cerebrospinal fluid (aCSF). After the electrode settled (~15 min), mice performed a visual spatial detection task for ~2 h.[45] At the end of the behavioral sessions, mice were presented black and white visual stimuli to map spatial receptive fields (described below); we focused on these datasets recorded at the end of behavioral sessions in trained mice to limit the effects of spontaneous behavioral variability in mice not performing visual tasks. Nevertheless, major findings regarding ON and OFF dominance from mice trained in behavioral tasks (Figures 1, 2, and 3A) were also evident in untrained mice (Figures 3B, 3C, and 4). As a control for any possible effects of training, combining recordings from both trained and passive awake mice (n = 94) did not diminish strong OFF dominance in binocular V1 (p < *0.001;* sign test), nor ON/OFF balanced responses in monocular V1 (n = 50; p = *0.04*, sign test*)*. Furthermore, recordings in LGN from awake mice untrained in visual tasks showed concordant spatial biases in ON/OFF responses.

Haider lab—LGN extracellular

LGN recording sites were targeted with stereotaxic coordinates (−2.5 mm posterior to bregma −2.5 mm lateral from midline). Mice were habituated for a minimum of 3 days to the recording environment prior to experimentation. Single shank electrodes (Neuro-nexus, A1x32-Poly-3) were used to record from LGN. While advancing the electrode, full screen flash stimuli were shown at 2, 4, and 8 Hz, and unit responses were assessed on-line to determine whether the electrode was in LGN (~3mm below the dura). The

electrode was inserted only once per recording session, and in most instances confirmed with histology. Mice were shown black and white square stimuli (see below) to map spatial receptive fields.

For V1 and LGN recordings using Neuronexus probes, electrical signals were acquired through a Cereplex Direct (Blackrock Microsystems). Raw neural signals were acquired at 30 kHz. Local field potentials (LFP) were band pass filtered at 0.3-200Hz. V1 layers were identified via current source density analysis[44] (Figure S1).

Haider Lab—V1 whole-cell patch-clamp recordings

We made whole-cell patch-clamp recordings from excitatory pyramidal neurons of awake (n = 9) and anesthetized mice (n = 10), as detailed previously.[33] We used the exact same stimulus protocol (detailed below) to record whole-cell and extracellular silicon probe responses, with no additional fine-tuning of stimuli during whole-cell recordings. We observed no significant differences in ON/OFF dominance within spatial location for awake versus anesthetized V_m recordings, so these were combined within location (Awake versus anesthetized SNR log ratios monocular: 0.07 ± 0.1 versus 0.05 ± 0.2, p = 0.6; binocular: −0.04 ± 0.2 versus −0.05 ± 0.2; p = 0.8, Wilcoxon rank sum tests; median ± IQR). We also observed no change to V_m results if we excluded a single binocular neuron recorded from a CNTNAP2$^{−/−}$ mutant mouse (Full population median V_m SNRs [White, Black]: [2.16, 3.31]; After exclusion: [2.17, 3.22]; p < 0.001 for both datasets), or if we excluded 2 monocular neurons recorded from a mouse of uncertain genotype (Full population median V_m SNRs [White, Black]: [4.23, 3.39]; After exclusion: [4.65, 3.67]; p < 0.001 for both datasets).

Saleem lab—V1 and LGN extracellular

Seven days following the surgery mice underwent the first habituation session in the virtual reality apparatus. Following the habitation period (one session per day, 8-13 days), a ~1mm craniotomy was performed centered over V1 (2 mm lateral to sagittal midline and 0.5 mm anterior to lambda) or LGN (1.9 mm lateral and 2.4 mm anterior from lambda). Mice were allowed to recover for 4-24 h before the first electrophysiology recording session. Multiple recording sessions were executed from each animal (one per day, n = 37 recordings, min 2, max 9). To preserve the brain tissue we left the dura intact. This was pierced locally by the silicon probe (ASSY-37 E-1, Cambridge Neurotech Ltd.) at the beginning of each recording session. For LGN recordings, the probe was advanced to a depth of ~3 mm until visual responses to flashing stimuli were observed. Electrophysiology data were acquired with an Open-Ephys acquisition board[52] and units were isolated using Kilosort.[49] Mice were free to run while presented black and white visual stimuli to map spatial receptive fields (described below).

Visual stimuli

Haider lab—Visual stimuli

We used LCD displays (Dell Ultrasharp U2417H or U2419H) with peak luminance of 250 cd * m^{-2}. Experiments used 2 displays positioned at right angles to one another (Figure 1), such that stimuli at 0° and 90° have a similar viewing angle relative to the axis of the mouse eye. This configuration minimizes (but does not eliminate) potential confounds of LCD panels and viewing angle. To confirm linearization, we displayed stimuli across the full range of pixel intensities (full black to full white), and measured the resulting monitor luminance values with a photodiode (Thorlabs), and then corrected this relationship with the (inverse) exponential function. We measured light levels using a photometer (AEMC CA811) with spectral sensitivity range (500 – 620 nm) overlapping the peak absorption wavelengths for both rods and M-cones, positioned at the same viewing angle as the mice (Figure 1). Averaged across all monitors (±SD), stimuli at [100% black, 50% gray background, 100% white] stimuli provided [0, 117.5 ± 14.4, 237.3 ± 28.7] cd * sr * m^{-2}. Mice viewed vertical bars at various contrasts and spatial locations (Figure 1). Bars were 9° wide and covered the whole height of the screen (spanning 50°). Bars were shown at 17 locations covering binocular and monocular areas of visual space, spaced evenly every 9.6° from −37.8° to 115.8° azimuth. The vertical meridian was defined as 0°. Contrasts ranged from 100% black to 100% white. Pixel values ranged from 0-255, and gray was set at 128. Michelson contrast was calculated as percent pixel value difference from gray background with the following equation:

$$contrast = \frac{pixel - grey}{grey} * 100$$

Each stimulus lasted 0.1 s before disappearing, and subsequent stimuli appeared after 0.3 s of gray screen. Stimuli were shown 10 times for each polarity, contrast, and location. Contrasts levels were 5, 10, 25, 40, 50, 75, and 100% for both black and white, but not all contrasts were shown in all sessions. Stimulus sequences were randomized for location, polarity, and contrast. The stimuli used to map receptive fields for LGN experiments consisted of black (minimum luminance) and white (maximum luminance) squares presented individually against a gray background of mean luminance. The squares were 7° in width and appeared in one of 160 spatial locations spanning 90° x 50°. Squares were presented for 0.1 s, followed by 0.3 s of gray screen before the appearance of the next square. Each square was presented in a randomized spatial location and color value per trial, with ten trials per color per location.

Saleem lab—Visual stimuli

Awake mice were shown a series of sparse noise frames consisting of a 9x9 (10° squares) or 8x8 grid (15° squares). The squares could each independently be black, gray or white. Stimuli were gamma-calibrated by displaying them across the full range of pixel intensities (full black to full white on gray background), measuring luminance with a photometer (Konica Minolta CS-100a) from mouse viewing angle at 0°, then linearizing the relationship between pixel intensity and luminance. The luminance for full black and white stimuli were 1.2 ± 0.4 and 33.6 ± 1.3 cd * m^{-2}, respectively. Only five squares could either be white or black at any frame presentation. Frames were shown for 0.1 s each in immediate succession. A single session lasted five minutes, or 3000 frames. Frame sequence was used posteriorly to construct a neural response to black, white, and gray stimuli in each square location.

Allen Institute—Visual stimuli

Detailed stimulus parameters are described elsewhere.[51] Briefly, awake mice were shown a variety of stimuli in blocks. A receptive field mapping stimulus (20° drifting grating, 0.25 s duration, 0.04 cycles per degree; 2 Hz temporal frequency) appeared at a single randomly chosen location on the screen (forming a 9 × 9 grid) tiling the whole visual field. Stimuli also included full-field flashes of black and white (0.25 s duration, 2 s inter-trial interval with uniform gray screen).

Data was retrieved from the Allen Institute Visual Coding – Neuropixels database using their proprietary SDK. Data was compiled last on June 22, 2020. For each unit, spike times and the precomputed on/off ratio (ratio of mean responses during 0.25 s) were retrieved. Detailed instructions for accessing the database and recording sessions (n = 47) and analysis code have been publicly deposited (see Key Resources Table) and linked from the lead contact's institutional website.

The table below summarizes the datasets, stimulus properties, and results in each figure.

Lab	Area	Recording method	Stimulus	Size (W x H)	Duration	ISI	Main Figure *(Supplemental Figure)*
Haider	V1	Neuronexus (32ch)	Flashed bars	9° x 50°	0.1 s	0.3 s	Figure1-2, 3A *(Figures S1A–S1F,H,I; S2; S3A-B, D-E)*
Saleem	V1	Cambridge Neurotech (32ch)	Flashed squares	9° x 9° or 15° x 15°	0.1 s	0.1 s	Figure 3B
Haider	LGN	Neuronexus (32ch)	Flashed squares	7° x 7°	0.1 s	0.3 s	Figure 3C *(Figures S4A and S4B)*
Saleem	LGN	Cambridge Neurotech (32ch)	Flashed squares	15° x 15°	0.1 s	0.1 s	Figure 3D *(Figures S4C and S4D)*
Haider	V1	Whole-cell patch-clamp	Flashed bars	9° x 50°	0.1 s	0.3 s	Figure 4 *(Figure S1G; S4F-G)*
Haider	V1	Neuropixels 1.0	Flashed bars	9° x 50°	0.1 s	0.3 s	*(Figure S3F)*
Allen Inst.	V1	Neuropixels 1.0	Full screen flash	120° x 95°	0.25 s	2 s	*(Figure S3C)*
Haider	V1	Neuropixels 1.0	Full screen flash	188° x 50°	0.25 s	2 s	*(Figure S3F)*
Haider	V1	Neuronexus probes (A32)	Full screen flash	188° x 50°	0.25 s	2 s	*(Figure S3E)*

QUANTIFICATION AND STATISTICAL ANALYSIS

Spike sorting
Haider lab—Spike sorting
Single unit activity (V1 Neuronexus recordings) was isolated with a semi-automated sorting algorithm[48] as detailed previously,[44] or with Kilosort[49] for LGN recordings and Neuropixels 1.0 recordings (IMEC) as previously described.[53] We classified single units as fast-spiking (FS, waveform peak-to-trough < 0.57ms) and regular spiking (RS, peak-to-trough > 0.57 ms) based on their waveform widths (Figure S3). FS neurons in mice are predominantly parvalbumin (PV) positive inhibitory neurons, while > 85% of RS neurons are putative excitatory neurons.[54]

Saleem lab—Spike sorting
Single units were isolated using Kilosort.[49] We selected only units that had a mean firing rate greater than 0.5 Hz in the first and last third of the sparse noise presentation period.

Allen Institute—Spike sorting
Neurons in the Allen Institute dataset were pre-sorted and packaged with several pre-computed quality metrics, as detailed elsewhere.[51] We plotted histograms of spike waveform widths and observed a clear bimodal distribution with a natural partition at 0.42 ms, and used this to classify RS and FS groups.

Vm analysis—Haider lab
Detailed methods have been described previously.[33,45] Whole-cell patch-clamp recordings were performed in current clamp mode (Molecular Devices, Multiclamp 700B) and acquired at 20 kHz with custom software (MATLAB). All recordings were in L2/3 based on depth estimated from the micromanipulator. Visual stimuli were displayed as described above, but only at 100% contrast. In some cases neurons only emitted spikes for bars of one color, so calculations for log ratios were assigned SNR = 1 for the bar color with no spikes.

Receptive field (RF) map analysis
Haider lab—V1 RF analysis
Recording sites in V1 were targeted with stereotaxic coordinates and/or intrinsic signal imaging, and further verified with functional localization of visual spatial receptive fields. A receptive field (RF) map for each recording session was created by first averaging together the LFP responses per electrode channel across all stimulus contrasts per stimulus location. This resulted in a 3D matrix of LFP responses: [stimulus location x time x probe channel]. Note that a sliding window was not used for RF map construction (*cf.* Saleem lab – V1 RF analysis). The median response across probe channels (averaging across laminar depth) generated a global

map of spatial responses for each azimuth location across time. The stimulus position that evoked the largest LFP activation (depth negative voltage response; see Figure 1) was designated as the central location of the receptive field (RF). Recordings with central RF locations < 40° in azimuth were classified as binocular recordings (RF preference: 19.8 ± 7.1°, median ± MAD, n = 58) whereas those with preferred location > 55° were classified as monocular (RF preference: 77.4 ± 8.5°, n = 36). This categorization is broadly consistent with anatomical and physiological definitions of the binocular and monocular representations in mouse V1.[55,56] Here we focused on responses elicited by 100% contrast black or white stimuli, since these were the most reliable and comparable across recordings (Figure S2). For spiking data, RF maps were calculated as described above for each neuron. Spiking in each stimulus location was binned every 20 ms to create a peri-stimulus-time-histogram (PSTH) in each location. PSTHs were then combined to form a space x time firing rate map for each neuron. Singular value decomposition (SVD) was used to automate the RF localization process for spiking maps due to quantity. SVD reduces RF maps to two 1-D components, and the maximum value of the spatial component is designated as the central RF location. These single neuron RF locations were verified by comparison to the RF location reported by the LFP during the same recordings. Experiments in Figure S3 D-F used SVD as above, and/or manual identification of best location in the RF location.

Haider lab—LGN RF analysis

A RF map for each neuron was created by generating a 2D histogram of spike counts for each neuron at each of the 160 spatial locations. The mean response between 0.04 - 0.14 s after stimulus onset was taken for each unit to create a receptive field map.[30] A chi-square test for independence was used to determine the presence of a significant (p < 0.05) receptive field.[16]

Saleem lab—V1 RF analysis

Receptive field mapping was performed in awake mice free to run or rest on a treadmill (polystyrene wheel) in a virtual reality environment.[50] Black and white squares were projected in a 2-D grid pattern inside a demispherical dome that spanned 240° in azimuth and 120° in elevation on the right visual field. For a particular square stimulus location and color (i.e., a frame), a sliding window of 100 ms was used to bin spikes into discrete time points relative to stimulus onset. Time bins started at 10 ms prior to stim onset, and ended at 120 ms after stimulus onset, in intervals of 10 ms (14 time points). For example, the bin starting at 50ms would contain all spikes from 50-150 ms relative to stimulus onset. At each time point, an RF map (see above) was created by combining the responses to all squares in the 9x9 (10° squares) or 8x8 (15° squares) grid into one large response. For every neuron, the response map with the highest variance was selected in time – one for each black response and white response. These two maps were used for subsequent analyses. SVD was performed on each map, black and white independently, to determine the location of the best response in azimuth and elevation. Selection criteria were instituted specifically on this dataset with 2-D stimuli. Neurons with firing rate < 1 spike/s at the best location for both the black and white response were not analyzed. We next calculated for each neuron and for each stimulus color the percentage of locations in the RF map where normalized activation was > 0.7 of the global max firing rate. Neurons where > 40% of the map exceeded this threshold in both black and white response (i.e., there was no spatially localized RF) were excluded. Visual inspection of included neurons showed clear RFs. Stimulus locations where normalized activation was > 0.9 of the global max response were all expected to be within 1 location (±10° or ± 15°) of the maximum response location. Neurons with normalized activation > 0.9 of the global max response at non-contiguous spatial positions in both black and white RF maps were excluded. We note that applying selection criteria for the combined ON and OFF responses prevented exclusion of neurons that were strongly responsive to one color, but not at all responsive to the other color. We then sorted neurons into binocular versus monocular groups by best azimuthal RF locations, using the same criteria as before, and calculated SNR and $\log_{10}$ transformed ratios for each stimulus color as described previously.

Saleem lab—LGN RF analysis

Receptive field maps of LGN neurons were computed in the same way as V1 neurons, but only 15° flashing squares (8x8 grid) were used.

Allen Institute—V1 RF analysis

This dataset was pre-processed by the Allen Institute to pass several quality metrics and quantify visual feature selectivity. The dataset precomputes optimal azimuthal receptive field location for each neuron, which we used to separate cells into binocular (−45 to 45°) and monocular (55° to 130°) groups. Full-field black or white flashes were used to calculate the ON/OFF response ratio for each cell as the mean firing rate during "ON" presentations divided by the mean firing rate during "OFF" presentations. A $\log_{10}$ transform was applied to these precomputed ratios just like all other datasets (see Figure S3).

V1 laminar identification—Haider lab

Laminar LFP responses were separated by using current source density analysis (Figure S1). We defined L4 to span ± 100 microns around the location of the earliest and largest CSD sink, consistent with prior functional and anatomical localization of L4 in mouse V1.[30,45] After designating L4, the other layers (L2/3, L5/6) were analyzed by taking the median across channels within layer. Neurons were assigned to specific layers based on the location of the channel with the largest amplitude spike waveform. Spike analysis for all datasets combined neurons across layers because of unequal sampling, and because there was no clear indication of unique laminar profiles in LFP analysis (Figure 2).

SNR calculation

We quantified ON versus OFF dominance using previously established methods.[8] Raw LFP and spiking traces were converted into signal-to-noise ratio (SNR) traces. SNR was calculated as

$$SNR = \frac{peak\,response - mean(baseline)}{std(baseline)}$$

where baseline represents the response during the pre-stimulus period (global activity level in the -0.1 s preceding stimulus onset for all stimulus locations). For single-unit data, if the standard deviation of the baseline equalled 0 (no activity), the SD (baseline) component was artificially set at 1. The raw response was calculated differently for LFP versus single-unit data. For LFP, the raw response was the mean of the preferred center location $\pm$ 1 adjacent locations. Since spike RFs are narrower than LFP RFs,[33] the peak response for spike RFs was calculated as the max (not mean) across the center $\pm$ 1 locations . In all cases, conversion to SNR resulted in a trace of response amplitude normalized by the SD. To quantify responses to black and white stimuli, we computed a metric based on the $\log_{10}$ ratio of the responses to white stimuli versus black stimuli, consistent with previous studies:[8]

$$SNR\ ratio = \log_{10}\left(\frac{SNR_{white}}{SNR_{black}}\right)$$

We defined the time point of SNR ratio calculation by identifying the max SNR value of the mean trace (LFP or V_m) or PSTH (spikes) that combined black and white responses. Identification of the overall max SNR was restricted to a window spanning the earliest visual response latency in V1 (Figure S1; LFP data: 30-100ms after stimulus onset; spiking data: 0-180ms; V_m data: 0 – 200ms). For spike analysis (Haider Lab data), each time point of the PSTH contained spikes binned at 20 ms (see Haider Lab -V1 RF Analysis). The max SNR time points identified for spike data captured stimulus response onsets rather than offsets (mean latency: 86 $\pm$ 30 ms ($\pm$SD), n = 1086 spike SNR responses). Only 11% of identified max SNR responses occurred at $\geq$ 140 ms, the earliest conceivable offset response to a 100 ms stimulus. Since the PSTH was binned at 20 ms (Haider lab data), this max SNR value captured spikes within 20ms of the peak response. The SNR ratio was then computed at this same latency using responses for each bar color, then $\log_{10}$ transformed as described above. $\log_{10}$ SNR ratios < 0 were classified as OFF, while those > 0 were classified as ON. The results were unaffected if we took the max SNR values of each stimulus polarity at their respective peak latencies, or if we restricted identification of max SNR times to £ 100 ms for spikes (Figure S1); similarly, in whole cell recordings, restricting identification of peak spike or V_m responses to < 150ms (Figures 4H and 4I) did not affect the results. For silicon probe recordings, neurons with either white or black SNR = 0 (single polarity responders) were excluded. This method was used for both V1 and LGN neurons in all datasets. For the Allen Institute dataset, ON-OFF ratios were pre-computed,[51] and these were used for the above equation.